NANO LETTERS

Letter

pubs.acs.org/NanoLett

Determination of Energy Level Alignment and Coupling Strength in 4,4′-Bipyridine Single-Molecule Junctions

Taekyeong Kim,[†] Pierre Darancet,[†,‡] Jonathan R. Widawsky,[†] Michele Kotiuga,[‡,∥] Su Ying Quek,[§] Jeffrey B. Neaton,*[,‡,∥] and Latha Venkataraman*[,†]

[†]Department of Applied Physics and Applied Mathematics, Columbia University, 500 W. 120th Street, New York, New York 10027, United States

[‡]Molecular Foundry, Materials Sciences Division, Lawrence Berkeley National Laboratory, Berkeley, California 94720, United States

[§]Department of Physics, Graphene Research Centre and Centre for Computational Science and Engineering, National University of Singapore, 21 Lower Kent Ridge Rd, Singapore 119077, Singapore

[∥]Department of Physics, University of California, Berkeley, Berkeley, California 94720, United States

Supporting Information

ABSTRACT: We measure conductance and thermopower of single Au−4,4′-bipyridine−Au junctions in distinct low and high conductance binding geometries accessed by modulating the electrode separation. We use these data to determine the electronic energy level alignment and coupling strength for these junctions, which are known to conduct through the lowest unoccupied molecular orbital (LUMO). Contrary to intuition, we find that, in the high-conductance junction, the LUMO resonance energy is further away from the Au Fermi energy than in the low-conductance junction. However, the LUMO of the high-conducting junction is better coupled to the electrode. These results are in good quantitative agreement with self-energy corrected zero-bias density functional theory calculations. Our calculations show further that measurements of conductance and thermopower in amine-terminated oligophenyl−Au junctions, where conduction occurs through the highest occupied molecular orbitals, cannot be used to extract electronic parameters as their transmission functions do not follow a simple Lorentzian form.

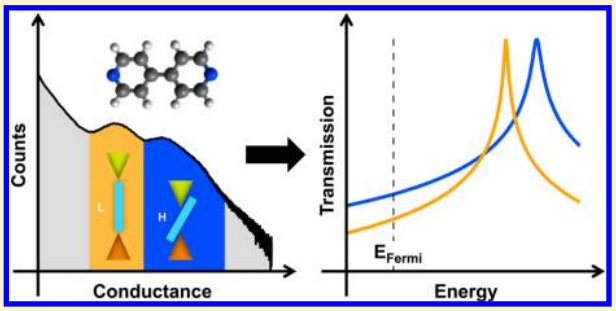

KEYWORDS: *Level alignment, electronic coupling, single-molecule junctions, conductance switching, thermopower*

Quantities that control the transport properties of organic-based devices at the nanoscale are the electronic coupling of frontier molecular orbitals to the metal electrodes and the alignment of their energy levels relative to that of the metal Fermi level (E_F).[1,2] Determining electronic molecular energy level alignment ($\Delta E = E_{resonance} - E_F$) and coupling strength (Γ) at metal/organic interfaces is thus critical to the design and development of tunable metal−molecule−metal devices.[3−5] The ionization potential (IP) and electron affinity (EA) of molecules in gas-phase, in solution, and in self-assembled monolayers on metals have been measured using a variety of spectroscopic tools.[6−9] However, the electronic structure of a molecule bonded to two electrodes cannot currently be determined by conventional spectroscopy; further, it cannot be deduced from gas-phase measurements, since the junction geometry and environment leads to hybridization due to bonding, the formation of interface dipoles, and large static polarization effects, all of which impact level alignment.[9−15] Therefore, a quantitative determination of ΔE and Γ is not easily accomplished.

Here, we directly determine ΔE and Γ for single-molecule junctions formed with 4,4′-bipyridine (BP) at low bias voltages by simultaneously measuring conductance (G) and thermopower (S) using the scanning tunneling microscope based break-junction technique (STM-BJ). ΔE and Γ are measured for high conductance (high-G) and low conductance (low-G) junctions in sequence in a single trace through repeated junction elongation and compression. We find that high-G junctions exhibit both larger ΔE and Γ compared to low-G junctions. The values determined here for ΔE and Γ are in excellent quantitative agreement with self-energy corrected density functional theory calculations. Finally, our calculations show that measurements of G and S for amine-terminated oligophenyl−Au junctions cannot be used to determine ΔE and Γ as their transmission functions cannot be represented by a single Lorentzian.

The thermopower, or the Seebeck coefficient, $S = -\Delta V/\Delta T$, is the ratio of potential, ΔV, that develops across the junction when a temperature difference, ΔT, is present.[16] S can be determined by measuring the open circuit voltage (ΔV, with $I =$

Received: November 7, 2013
Revised: January 6, 2014
Published: January 21, 2014

   dx.doi.org/10.1021/nl404143v | *Nano Lett.* 2014, 14, 794−798

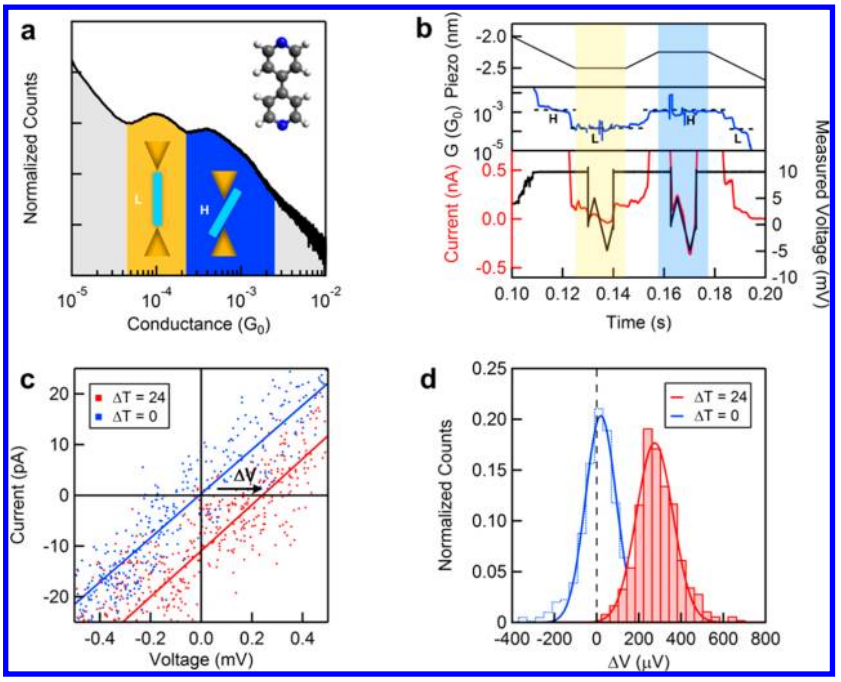

Figure 1. (a) Normalized linear-binned one-dimensional conductance histogram for 4,4′-bipyridine (inset is the BP structure). The histogram is constructed without any data selection from 20 000 traces measured at a 25 mV bias voltage using a linear conductance bin size of 1×10^{-5} G_0. The blue (yellow) regime highlights the high-G (low-G) geometry. (b) Single sample trace of a BP low-G junction that is compressed to yield a high-G junction. The upper panel shows the piezo ramp, the middle panel shows the conductance, and the lower panel shows the measured current (left axis) and voltage (right axis). The colored shaded regions indicate the two "hold" sections. The high-G and low-G conductance steps are also seen during the first pull section. (c) Sample IV curves measured with $\Delta T = 24$ K (red) and with $\Delta T = 0$ K (blue) on the BP high-G junction. The lines are the linear fits to the raw data (dots). The open circuit voltage (ΔV) is positive which gives a negative thermopower. (d) Normalized histograms for ΔV of the BP high-G junction at $\Delta T = 24$ K (red) and $\Delta T = 0$ K (blue) are shown along with Gaussian fits.

0) or the closed-circuit current (I, with $V = 0$) while maintaining a temperature difference across the junction.[17−19] For coherent tunneling through a single molecule junction, and in special cases when the transmission function is well-described by a single Lorentzian line shape peaked at an energy ΔE from E_F, with a full width at half-maximum of Γ, a concurrent measurement of G and S for a single molecule junction allows the determination of both ΔE and Γ as[16,20]

$$\Delta E = -2\frac{S_0}{S}\left(1 - \frac{G}{G_0}\right) \qquad \Gamma = 4\frac{S_0}{S}\sqrt{\frac{G}{G_0}\left(1 - \frac{G}{G_0}\right)} \tag{1}$$

where $G_0 = 7.74 \times 10^{-5}/\Omega$ and $S_0 = 7.25$ eV $\times 10^{-6}$ V/K at 300 K.[21]

We first measure the conductance of BP by repeatedly forming and breaking Au point contacts in the presence of molecules with a modified STM-BJ setup[22] that has been described in detail previously.[23] BP is deposited on the gold substrate from an acetone solution, the solvent is allowed to evaporate, and 20 000 conductance traces are measured over a period of 5 h. The linear binned conductance histogram generated from these traces, without any data selection, is shown in Figure 1a (no temperature difference is applied here). It has two peaks, a low-G peak at $\sim 1 \times 10^{-4}$ G_0 (yellow) and a high-G peak at $\sim 4 \times 10^{-4}$ G_0 (blue) due to two different molecular junction geometries. The low-G geometry has the molecule extended between the two electrodes and bonded with the N−Au bonds perpendicular to the conducting π-system, while the high-G geometry has the molecule tilted between the electrodes as shown in the insets of Figure 1a.[24]

We measure S following a procedure detailed previously,[18,19] where the substrate temperature is controlled by a Peltier heater, and the tip is kept close to room temperature. IV curves are measured while holding the electrode separation fixed, and the intercept of the IV curve at zero current determines the ΔV for this junction, which yields S, knowing ΔT. Furthermore, the slope of the IV curve, $\Delta I/\Delta V$, determines the junction conductance in the linear response regime.

The measurements with BP carried out here are designed to probe, in the same junction, ΔE and Γ of the low-G and high-G states. We therefore need to measure G and S for both molecular junction geometries in the same trace. This is carried out by measuring IV curves while applying a modified piezo ramp that includes segments when the substrate is held fixed relative to the tip (black solid trace in upper panel in Figure 1b), while also applying a ΔT across the junction. This ramp first pulls the Au point-contact apart by 2.5 nm, holds the electrodes fixed for 20 ms, then pushes the electrodes together by 0.2 nm followed by a second 20 ms hold before the final pull. During each "hold" portion, an IV curve is measured using a voltage range of ±5 mV (bottom panel in Figure 1b, red and black lines). We measure 50 000 traces with this ramp and select those where the first hold has a low-G geometry that is compressed to yield a high-G geometry during the second hold. These traces are selected by analyzing the conductance during each hold segment. A sample conductance trace is shown in middle panel (blue solid trace) in Figure 1b. A large fraction of the traces show junctions that either start in the high-G configuration or are broken prior to the hold and cannot be analyzed further, and overall, we find that about ∼800 traces follow this trajectory.

dx.doi.org/10.1021/nl404143v | Nano Lett. 2014, 14, 794−798

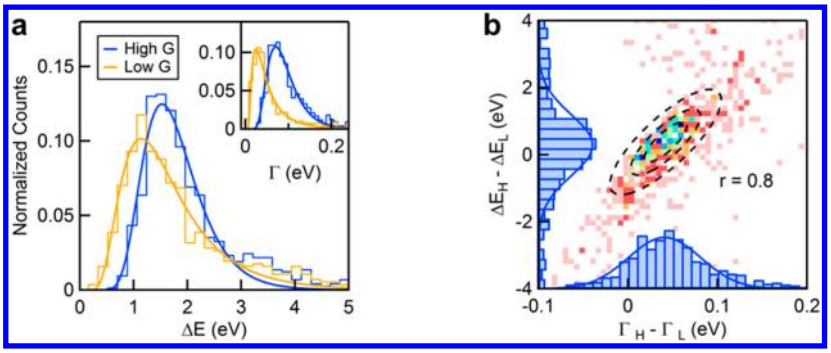

Figure 2. (a) Normalized histograms of resonance energy position relative to E_F (ΔE) for high-G (blue) and low-G (yellow) junctions of BP. The inset shows histograms of coupling strengths (Γ) for each geometry. The solid lines are log-normal fits. (b) Correlation plot for the change of resonance energy ($\Delta E_H - \Delta E_L$) and the change of coupling strength ($\Gamma_H - \Gamma_L$) for high-G and low-G junctions in each individual junction. The cross-correlation parameter r is 0.8. The peaks from the histogram of the changes are 0.35 eV for ($\Delta E_H - \Delta E_L$) and 0.04 eV for ($\Gamma_H - \Gamma_L$).

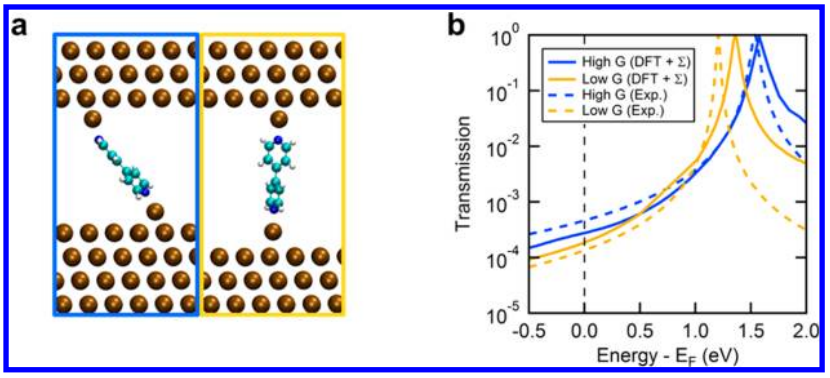

Figure 3. (a) Optimized structures of BP adatom junctions for high-G (blue box) and low-G (yellow box) geometries. Gold, pale blue, blue, and white circles denote Au, C, N, and H, respectively. (b) Transmission functions calculated using the DFT+Σ method (solid lines) shown on a log scale for high-G (blue) and low-G (yellow) geometry of BP. Lorentzian curves generated from the experimental values of ΔE and Γ are shown as dashed lines for the high-G and low-G junctions.

Figure 1c shows two sample IV traces for BP in the high-G geometry measured at ΔT = 24 K (red) and at ΔT = 0 K (blue). The lines are the linear fits to the IV traces. We find that voltage offset at zero current, ΔV, is positive which yields a negative S, indicating that dominant orbital for transport is the lowest unoccupied molecular orbital (LUMO).[18] Figure 1d shows the histograms of ΔV's obtained by the high-G geometry with two different temperature gradients. From the Gaussian fit to this histogram, we get a mean ΔV of about 260 μV when ΔT is increased from ΔT = 0 to ΔT = 24 K which yields a S of −8.4 μV/K. Histograms of S and G (determined from the slope of the IV curve) for high-G and low-G geometries are shown in the SI, Figure S1.

We now use eq 1 above to determine ΔE and Γ, using G and S for each individual junction, and compile the results in Figure 2a for high-G junctions (blue) and for low-G junctions (yellow). The peaks of these distributions are at ΔE = 1.5 and 1.2 eV for the high-G and low-G junctions, respectively. The corresponding values for Γ (inset of Figure 2a) are 0.07 and 0.03 eV for high-G and low-G junctions. These results demonstrate experimentally that the high-G junction has a higher resonance (further away from E_F) when compared with that of the low-G junction despite a higher conductance consistent with calculations discussed below. The higher conductance results from a larger Γ, indicating a stronger electronic coupling.[24] This finding is not exclusive to BP. Indeed, we find a similar result from simultaneous measurements conductance and thermopower measurements for single-1,2-di(4-pyridyl)ethylene (BPE) molecular junctions which also has two LUMO-based conductance states.[18,25,26] (see SI, Figure S2 for data). We conclude that in general, for pyridine-linked molecules, the high-G junction will have a higher resonance position and stronger coupling compared to the corresponding low-G junction.[26,27]

We now use the measurements of ΔE and Γ for each BP junction that switches from a low-G state to a high-G state on compression to determine the change in the resonance position ($\Delta E_H - \Delta E_L$) and the change in coupling ($\Gamma_H - \Gamma_L$) in every trace. In Figure 2b, we plot $\Delta E_H - \Delta E_L$ against $\Gamma_H - \Gamma_L$ and overlay a cross-correlation analysis (dashed circles) as explained in the SI. We find a cross-correlation parameter r of 0.8. This implies that an increase in ΔE is strongly correlated with an increase in Γ when going from a low-G geometry to a high-G geometry.[24] This is consistent with a picture where the enhanced coupling in the high-G geometry enables charge back-donation from the Au to the molecule, which in turn results in a self-consistent shifting of the LUMO resonance upward and away from E_F due to electrostatic repulsion.

To determine both ΔE and Γ for representative high-G and low-G junctions and understand these measurements, we use first-principles calculations with a self-energy corrected, parameter-free scattering-state approach based density functional theory (DFT+Σ). We model the electrodes using two Au(111) slabs with seven layers of gold for the leads, using a 4 × 4 unit cell, and optimize the geometries using density functional theory (DFT) with a GGA (PBE) functional[28] and

dx.doi.org/10.1021/nl404143v | Nano Lett. 2014, 14, 794−798

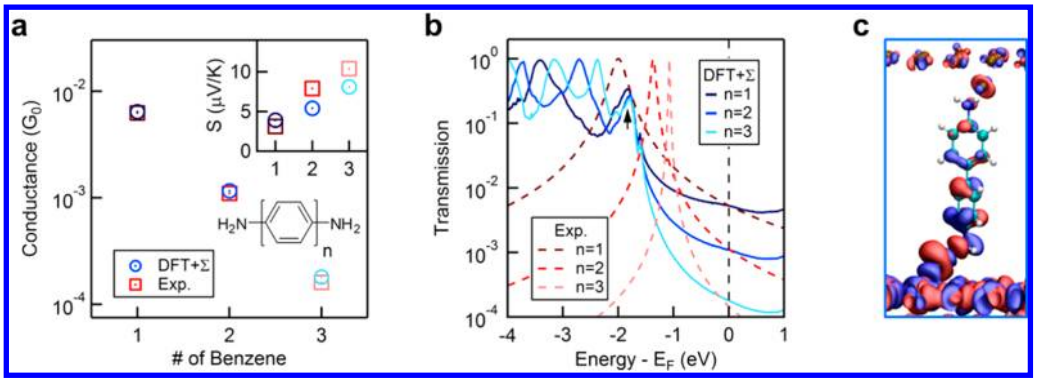

Figure 4. (a) Conductance against the number of benzene rings for amine-terminated oligophenyl–Au junctions. Inset: Thermopower against the number of benzene rings. (b) DFT+Σ transmission functions (solid lines) shown on a log scale for this series. Transmission curves generated using the experimental values of G and S assuming a single-Lorentzian model for all of oligophenyls are also shown as dashed lines. (c) Isosurface plot of the transmitted scattering state at −1.8 eV (indicated by arrow in b) for a biphenyl–diamine junction.

the SIESTA package[29] following an approach outlined in earlier works.[24,30−32] The starting geometries for the high-G and low-G junctions are adapted from an earlier work, where the high-G geometry corresponds to a shorter interelectrode distance. Undercoordinated adatom binding motifs are used on both sides for both of high-G and low-G geometries, following prior work.[32] The transmission functions are subsequently computed using a self-energy-corrected PBE Kohn–Sham Hamiltonian (DFT+Σ) for the calculation of the scattering-states of the junction (see SI for details), as implemented in the Scarlet code.[33]

Junction structures for high-G (blue box) and low-G (yellow box) geometries of BP with adatom motifs are shown in Figure 3a. The high-G geometry has a more tilted junction structure with a smaller interelectrode distance than the low-G geometry. Figure 3b compares the calculated transmission functions (solid lines) of BP for high-G junction (blue) and for low-G junction (yellow) with the Lorentzian curves (dashed lines) generated using the average ΔE and Γ determined from G and S measurements. We see that both experiment and DFT+Σ show that the increase in conductance results from an increase in Γ, the width of the LUMO resonance. We find that the computed DFT+Σ transmission function of the high-G junction with 1.57 eV for ΔE reproduces the experimental Lorentzian curve well. For the low-G junction, we find a deviation of 0.15 eV in the resonance position predicted by experiment from the calculated transmission. The slight non-Lorentzian form of the computed transmission function can explain this difference. Indeed, fitting the DFT+Σ transmission function in the region around E_F with a Lorentzian yields a ΔE of 1.20 eV for the low-G junction, which is in excellent agreement with the experimental value determined from low-bias measurements (see SI Figure S3 for the details).

We now contrast these results to measurements with amine-terminated molecules, which conduct through the highest occupied molecular orbital (HOMO) resonance.[32] We measure, in the same manner as described above, the G and S for a series of three amine-terminated oligophenyls with n = 1−3 phenyl rings and compare these to results from DFT+Σ calculations in Figure 4a and its inset.[31,34] We find good quantitative agreement between theory (circles) and experiment (squares) for both G and S. The calculated transmission functions (solid lines) for this series with adatom motifs of Au binding sites are shown in Figure 4b, where we see clearly that they deviate significantly from a simple Lorentzian form due to the peak around −1.8 eV as indicated by the arrow. Indeed, if we use eq 1 with the experimental G and S to determine ΔE and Γ (see SI, Figures S4, S5, and S6 for histograms) as for the pyridine system, we obtain the Lorentzian curves indicated by the dashed lines (Figure 4b), which deviate significantly from theory. The transmission feature at around −1.8 eV is associated with a strong hybridization of Au d-states of the undercoordinated Au binding sites and the HOMO resonance as seen in the isosurface plot of the scattering states shown in Figure 4c for the biphenyl junction.[31] Due to the presence of these d-states, the coupling of the Au electrodes to the molecular orbitals is highly energy-dependent on the occupied side, and the transmission function differs significantly from a Lorentzian form. Note that, in these systems, the lowest unoccupied orbital that couples to the Au states is much further away from E_F than the HOMO.[31] A meaningful constant Γ and ΔE cannot be extracted from experimental conductance and thermopower as done above for the pyridine systems. In general for junctions with Au electrodes, we expect the present breakdown of the Lorentzian model, and its consequence on extracting ΔE and Γ, to apply to all HOMO-conducting junctions (when LUMO is further away from E_F) when the resonance is deeper than the location of the Au-d states of the undercoordinated Au binding sites (around −1.8 eV).[35] In contrast, for molecules that conduct through unoccupied levels, such as the pyridines studied above, the Au density of states is approximately uniform due to their s–p character, which results in a Lorentzian shape for the LUMO transmission peaks.

In conclusion, we have determined the electronic level alignment and coupling in single-molecule junctions formed with 4,4′-bipyridine molecular junctions with measurements of G and S in a linear response regime. We find that the LUMO resonance energy is higher but better coupled in the high-G regime, while it is lower but more weakly coupled in the low-G regime. Both the resonance positions and their coupling are in excellent quantitative agreement with self-energy corrected zero-bias DFT calculations. We show however that these parameters are not easily determined for HOMO-conducting molecule–Au junctions due to the variation in the density of states of Au with energy below E_F.

■ ASSOCIATED CONTENT

Supporting Information

Additional information, methods, and figures. This material is available free of charge via the Internet at http://pubs.acs.org.

dx.doi.org/10.1021/nl404143v | Nano Lett. 2014, 14, 794−798

AUTHOR INFORMATION

Corresponding Author

*E-mail: lv2117@columbia.edu; jbneaton@lbl.gov.

Notes

The authors declare no competing financial interest.

ACKNOWLEDGMENTS

This work was supported primarily by the NSF MIRT program under award the DMR-1122594. Portions of this work were performed at the Molecular Foundry and supported by the Division of Materials Sciences and Engineering (Theory FWP), both under the auspices of the Office of Basic Energy Sciences of the U.S. Department of Energy under contract no. DE-AC02-05CH11231. We thank the National Energy Research Scientific Computing center for computational resources.

REFERENCES

(1) Ishii, H.; Sugiyama, K.; Ito, E.; Seki, K. *Adv. Mater.* **1999**, *11* (8), 605−625.

(2) Braun, S.; Salaneck, W. R.; Fahlman, M. *Adv. Mater.* **2009**, *21* (14−15), 1450−1472.

(3) Song, H.; Kim, Y.; Jang, Y. H.; Jeong, H.; Reed, M. A.; Lee, T. *Nature* **2009**, *462* (7276), 1039−43.

(4) Kim, Y.; Hellmuth, T. J.; Sysoiev, D.; Pauly, F.; Pietsch, T.; Wolf, J.; Erbe, A.; Huhn, T.; Groth, U.; Steiner, U. E.; Scheer, E. *Nano Lett.* **2012**, *12* (7), 3736−3742.

(5) Halik, M.; Klauk, H.; Zschieschang, U.; Schmid, G.; Dehm, C.; Schutz, M.; Maisch, S.; Effenberger, F.; Brunnbauer, M.; Stellacci, F. *Nature* **2004**, *431* (7011), 963−966.

(6) Dell'Angela, M.; Kladnik, G.; Cossaro, A.; Verdini, A.; Kamenetska, M.; Tamblyn, I.; Quek, S. Y.; Neaton, J. B.; Cvetko, D.; Morgante, A.; Venkataraman, L. *Nano Lett.* **2010**, *10* (7), 2470−2474.

(7) Zangmeister, C. D.; Robey, S. W.; van Zee, R. D.; Kushmerick, J. G.; Naciri, J.; Yao, Y.; Tour, J. M.; Varughese, B.; Xu, B.; Reutt-Robey, J. E. *J. Phys. Chem. B* **2006**, *110* (34), 17138−17144.

(8) Kahn, A.; Koch, N.; Gao, W. Y. *J. Polym. Sci., Part B: Polym. Phys.* **2003**, *41* (21), 2529−2548.

(9) Kim, B.; Choi, S. H.; Zhu, X. Y.; Frisbie, C. D. *J. Am. Chem. Soc.* **2011**, *133* (49), 19864−19877.

(10) Perrin, M. L.; Verzijl, C. J. O.; Martin, C. A.; Shaikh, A. J.; Eelkema, R.; Van Esch, J. H.; Van Ruitenbeek, J. M.; Thijssen, J. M.; Van Der Zant, H. S. J.; Dulić, D. *Nat. Nanotechnol.* **2013**, *8* (4), 282−287.

(11) Moth-Poulsen, K.; Bjornholm, T. *Nat. Nanotechnol.* **2009**, *4* (9), 551−556.

(12) Cahen, D.; Kahn, A. *Adv. Mater.* **2003**, *15* (4), 271−277.

(13) Kubatkin, S.; Danilov, A.; Hjort, M.; Cornil, J.; Bredas, J. L.; Stuhr-Hansen, N.; Hedegard, P.; Bjornholm, T. *Nature* **2003**, *425* (6959), 698−701.

(14) Heimel, G.; Romaner, L.; Bredas, J. L.; Zojer, E. *Phys. Rev. Lett.* **2006**, *96* (19), 196806.

(15) Heimel, G.; Romaner, L.; Zojer, E.; Bredas, J. L. *Nano Lett.* **2007**, *7* (4), 932−940.

(16) Paulsson, M.; Datta, S. *Phys. Rev. B* **2003**, *67* (24), 241403.

(17) Reddy, P.; Jang, S. Y.; Segalman, R. A.; Majumdar, A. *Science* **2007**, *315* (5818), 1568−1571.

(18) Widawsky, J. R.; Darancet, P.; Neaton, J. B.; Venkataraman, L. *Nano Lett.* **2012**, *12* (1), 354−358.

(19) Evangeli, C.; Gillemot, K.; Leary, E.; González, M. T.; Rubio-Bollinger, G.; Lambert, C. J.; Agraït, N. *Nano Lett.* **2013**, *13* (5), 2141−2145.

(20) Frisenda, R.; Perrin, M. L.; Valkenier, H.; Hummelen, J. C.; van der Zant, H. S. J. *Phys. Status Solidi B* **2013**, *250* (11), 2431−2436.

(21) Malen, J. A.; Doak, P.; Baheti, K.; Tilley, T. D.; Segalman, R. A.; Majumdar, A. *Nano Lett.* **2009**, *9* (3), 1164−1169.

(22) Xu, B. Q.; Tao, N. J. *Science* **2003**, *301* (5637), 1221−1223.

(23) Venkataraman, L.; Klare, J. E.; Tam, I. W.; Nuckolls, C.; Hybertsen, M. S.; Steigerwald, M. L. *Nano Lett.* **2006**, *6* (3), 458−462.

(24) Quek, S. Y.; Kamenetska, M.; Steigerwald, M. L.; Choi, H. J.; Louie, S. G.; Hybertsen, M. S.; Neaton, J. B.; Venkataraman, L. *Nat. Nanotechnol.* **2009**, *4* (4), 230−234.

(25) Aradhya, S. V.; Frei, M.; Hybertsen, M. S.; Venkataraman, L. *Nat. Mater.* **2012**, *11* (10), 872−876.

(26) Kamenetska, M.; Quek, S. Y.; Whalley, A. C.; Steigerwald, M. L.; Choi, H. J.; Louie, S. G.; Nuckolls, C.; Hybertsen, M. S.; Neaton, J. B.; Venkataraman, L. *J. Am. Chem. Soc.* **2010**, *132* (19), 6817−6821.

(27) Bagrets, A.; Arnold, A.; Evers, F. *J. Am. Chem. Soc.* **2008**, *130* (28), 9013−9018.

(28) Perdew, J. P.; Burke, K.; Ernzerhof, M. *Phys. Rev. Lett.* **1996**, *77* (18), 3865−3868.

(29) Soler, J. M.; Artacho, E.; Gale, J. D.; Garcia, A.; Junquera, J.; Ordejon, P.; Sanchez-Portal, D. *J. Phys.:Cond. Mat.* **2002**, *14* (11), 2745−2779.

(30) Darancet, P.; Widawsky, J. R.; Choi, H. J.; Venkataraman, L.; Neaton, J. B. *Nano Lett.* **2012**, *12* (12), 6250−6254.

(31) Quek, S. Y.; Choi, H. J.; Louie, S. G.; Neaton, J. B. *Nano Lett.* **2009**, *9* (11), 3949−3953.

(32) Quek, S. Y.; Venkataraman, L.; Choi, H. J.; Louie, S. G.; Hybertsen, M. S.; Neaton, J. B. *Nano Lett.* **2007**, *7* (11), 3477−3482.

(33) Choi, H. J.; Marvin, L. C.; Steven, G. L. *Phys. Rev. B* **2007**, *76* (15), 155420.

(34) Quek, S. Y. Q. S. Y.; Choi, H. J.; Louie, S. G.; Neaton, J. B. *ACS Nano* **2011**, *5* (1), 551−557.

(35) Widawsky, J. R.; Chen, W.; Vazquez, H.; Kim, T.; Breslow, R.; Hybertsen, M. S.; Venkataraman, L. *Nano Lett.* **2013**, *13* (6), 2889−2894.